Squeezed light from a laser with an internal $\chi^{(2)}$-nonlinear element

R. Schack, A. Sizmann, and A. Schenzle
Sektion Physik der Universität München, D-8000 München, Federal Republic of Germany
and Max-Planck-Institut für Quantenoptik, D-8046 Garching, Federal Republic of Germany
(Received 3 December 1990)

We present a theoretical investigation of the potential for squeezing of a doubly resonant cavity that contains a laser medium as well as a $\chi^{(2)}$ nonlinearity. If the lasing mode is coupled to its second harmonic, i.e., for a self-frequency-doubling laser, we find more than 60% squeezing in the up-converted mode outside the cavity. In the opposite case of a "self-down-converting laser," i.e., when the lasing mode is coupled to its subharmonic, a perfectly squeezed vacuum in the down-converted mode develops into a less squeezed state with a nonvanishing coherent amplitude as the pump rate is increased. Our analysis extends beyond the first stable regime of the classical dynamics and compares results for different laser models.

I. INTRODUCTION

In spite of recent progress in the generation of nonclassical states of light using semiconductor lasers,[1–4] there remain many good reasons for further investigating the potential for squeezing in conventional three- and four-wave-mixing experiments.[5–13] First of all, there is still no practical source of bright squeezed light, i.e., of squeezed light with a large coherent amplitude. Secondly, semiconductor lasers have a large linewidth and are not available for the whole range of wavelengths needed in optical experiments. And, last but not least, the investigation of squeezing in the optical parametric process is of considerable theoretical interest, since the definition of the squeezed state is intimately connected with the process of three-wave mixing.[14–16]

In a preceding letter,[17] we examined a theoretical model for a self-frequency-doubling laser, i.e., a laser with an intracavity χ^2-nonlinear crystal. We found that such a device could, in principle, produce more than 60% squeezing in the second-harmonic mode outside the cavity. To describe the laser medium, we used the standard laser model which was introduced independently by Haken[18] and Lamb.[19] In the meantime, we have become aware of parallel work[20,21] where a similar system is described using the laser model of Lax and Louisell[22] and where a maximum of 50% squeezing is predicted.

It is interesting to compare our previous results with those of Refs. 20 and 21. In these articles, the same general approach as that used in our letter is used. The model is formulated in terms of a Fokker-Planck equation for the diagonal P representation. Squeezing spectra are then obtained by a linearization around the stable fixed points of the classical-dynamical equations. The structure of the classical dynamics is independent of the particular laser model on which the analysis is based, as is shown in the present paper. The main difference between both laser models lies in the fluctuations. In the Haken-Lamb model, the diffusion coefficients in the Fokker-Planck equation grow linearly with the pump rate, whereas in the Lax-Louisell model, for a large pump rate, they approach a limiting value. This explains why, in the Haken-Lamb model, there is no squeezing in the first stable regime of the classical dynamics, whereas the analysis of Refs. 20 and 21—based on the Lax-Louisell model—yields 50% squeezing in this regime. The second stable regime of the classical dynamics, where our model predicts more than 60% squeezing, is not considered in Refs. 20 and 21.

The physical origin of the gain process suggests that the spontaneous-emission noise saturates far above threshold. This feature, which is absent in the Haken-Lamb model, is qualitatively contained in the Lax-Louisell model. On the other hand, the Haken-Lamb model is derived in a systematic expansion at the laser threshold,[23] whereas the Lax-Louisell model is mathematically inconsistent. It contains nonlinearities of arbitrary order, but only second-order derivatives. Close to threshold, both models agree. Up to the present time, there exists no experimental or theoretical investigation that decides which of the two models is a more accurate description of a laser far above threshold. Since squeezing depends in a subtle way on the fluctuations, terms of the order of the vacuum noise are important for the present analysis. Therefore, both models will be considered and the results will be compared.

In this article, the full potential for bright squeezing is evaluated by carrying out the analysis for all stable regimes of the classical dynamics. It turns out that nonclassical effects are enhanced if the cavity has a higher Q value for the lasing mode than for the converted mode, which corresponds to the condition of a low laser threshold. Strong squeezing can then be obtained in the converted mode outside the cavity. In Sec. II, this is shown for the self-frequency-doubling laser. The self-down-converting laser, which was also partially treated in Ref.

20, is examined as a source of bright squeezed light in Sec. III. In order to facilitate the comparison for both laser models, the structure of the classical dynamics is compiled in tables in a unified form. The potential for squeezing is displayed in diagrams for various values of the pump rate and the nonlinear coupling.

II. SELF-FREQUENCY-DOUBLING LASER

The model for the self-frequency-doubling laser introduced in Ref. 17 is based on the laser theory of Haken and Lamb. In the interaction picture, it is described by the following quasi-Fokker-Planck equation:

$$\frac{\partial P}{\partial t}=\left[-\frac{\partial}{\partial\beta_1}[\beta_1(\tilde{g}-\gamma_1-i\delta_1-b|\beta_1|^2)+\chi\beta_1^*\beta_2]+\text{c.c.}\right]P$$
$$-\left[\frac{\partial}{\partial\beta_2}\left[\beta_2(-\gamma_2-i\delta_2)-\frac{\chi}{2}\beta_1^2\right]+\text{c.c.}\right]P+\left[2\tilde{g}\frac{\partial^2}{\partial\beta_1\partial\beta_1^*}+\frac{\chi}{2}\left[\frac{\partial^2}{\partial\beta_1^2}\beta_2+\text{c.c.}\right]\right]P\ . \tag{1}$$

Here, $P(\beta_1,\beta_2)$ is the Glauber-Sudarshan P function, where β_1 and β_2 are the complex amplitudes of the intracavity fields in the fundamental and second-harmonic modes, respectively. We allow for detuning $\delta_1=\omega_1-\omega_L$ and $\delta_2=\omega_2-2\omega_L$ between the cavity modes and the lasing transition ω_L. These detunings are supposed to be adjusted to $\delta_2=2\delta_1$. The variables γ_1 and γ_2 are the cavity damping rates, $\tilde{g}$ is the pump parameter, b describes saturation of the lasing medium, and χ is the nonlinear coupling constant.

The corresponding equation based on the laser model of Lax and Louisell is

$$\frac{\partial P}{\partial t}=\left\{-\frac{\partial}{\partial\beta_1}\left[\beta_1\left[\frac{\tilde{g}}{1+b|\beta_1|^2/\tilde{g}}-\gamma_1-i\delta_1\right]+\chi\beta_1^*\beta_2\right]+\text{c.c.}\right\}P$$
$$-\left[\frac{\partial}{\partial\beta_2}\left[\beta_2(-\gamma_2-i\delta_2)-\frac{\chi}{2}\beta_1^2\right]+\text{c.c.}\right]P$$
$$+\left\{-\frac{1}{2}\left[\frac{\partial^2}{\partial\beta_1^2}\left[\frac{b\beta_1^2}{(1+b|\beta_1|^2/\tilde{g})^2}-\chi\beta_2\right]+\text{c.c.}\right]+\frac{\partial^2}{\partial\beta_1\partial\beta_1^*}\left[\frac{2\tilde{g}+b|\beta_1|^2}{(1+b|\beta_1|^2/\tilde{g})^2}\right]\right\}P\ . \tag{2}$$

As in Ref. 17, it is convenient to introduce scaled variables:

$$\tau=\gamma_2 t,\quad \alpha_i=\sqrt{b/\gamma_2}\beta_i\quad (i=1,2)$$
$$\Gamma=\frac{\gamma_1}{\gamma_2},\quad g=\frac{\tilde{g}}{\gamma_2},\quad \Delta=\frac{\delta_1}{\gamma_2}=\frac{\delta_2}{2\gamma_2},\quad \kappa=\frac{\chi}{\sqrt{b\gamma_2}}\ . \tag{3}$$

Equations (1) and (2) include phase diffusion. In this respect, our model of a self-frequency-doubling laser is more realistic than the usual model of second-harmonic generation,[24] where the external pump field is described by a stable classical wave.

A. Classical dynamics

Using the scaled variables Eq. (3), it is possible to write the classical equations of motion derived from the deterministic parts of Eqs. (1) and (2) in a unified form:

$$\dot{\alpha}_1=[\tfrac{1}{2}f_g(|\alpha_1|^2)-i\Delta]\alpha_1+\kappa\alpha_1^*\alpha_2\ ,$$
$$\dot{\alpha}_2=-(1+2i\Delta)\alpha_2-\frac{\kappa}{2}\alpha_1^2\ , \tag{4}$$

where the particular laser model enters through the function f_g:

$$f_g(x)=2(g-\Gamma-x)\quad\text{(Haken-Lamb)} \tag{5}$$

or

$$f_g(x)=\frac{2g}{1+x/g}-2\Gamma\quad\text{(Lax-Louisell)}\ . \tag{6}$$

The dot denotes derivation with respect to the dimensionless time τ. The classical equations of motion (4) are invariant under the transformation $(\alpha_1,\alpha_2)\rightarrow(\alpha_1 e^{i\phi},\alpha_2 e^{2i\phi})$ for an arbitrary angle ϕ. This phase symmetry suggests the definition of a reduced set of variables:

$$x_1=|\alpha_1|^2,\quad \alpha_1=\sqrt{x_1}e^{i\phi_1}\ ,$$
$$x_2=|\alpha_2|^2,\quad \alpha_2=\sqrt{x_2}e^{i\phi_2}\ , \tag{7}$$
$$x_3=\text{Re}(\alpha_1^2\alpha_2^*)=x_1\sqrt{x_2}\cos(2\phi_1-\phi_2)\ .$$

For a complete description of the system, the angle ϕ_1 may be used in addition to the variables x_1, x_2, and x_3. The phase symmetry now translates into the property that the equations of motion for x_1, x_2, and x_3 do not depend on the phase ϕ_1:

$$\dot{x}_1=f_g(x_1)x_1+2\kappa x_3\ ,$$
$$\dot{x}_2=-2x_2-\kappa x_3\ , \tag{8}$$
$$\dot{x}_3=[f_g(x_1)-1]x_3+2\kappa x_1x_2-\frac{\kappa}{2}x_1^2\ .$$

The equation for ϕ_1 reads

TABLE I. Self-frequency-doubling laser model characteristics for three fixed points.

Feature	Fixed point (i)	Fixed point (ii)	Fixed point (iii)
Stability range	$g<\Gamma$	$\Gamma<g<g_1$	$g>g_1$
Defining equations	$x_1=0$ $x_2=0$ $x_3=0$	$f_g(x_1)=\kappa^2 x_1$ $x_2=\kappa^2 x_1^2/4$ $x_3=-\kappa x_1^2/2$	$f_g(x_1)=1$ $x_2=x_1/4$ $x_3=-x_1/(2\kappa)$
Stability conditions	$f_g(x_1)<0$	$0<x_1<\dfrac{1}{\kappa^2}$	$x_1>\dfrac{1}{\kappa^2}$
Haken-Lamb equations		$x_1=\dfrac{1}{1+\kappa^2/2}(g-\Gamma)$ $g_1=\Gamma+\frac{1}{2}+\dfrac{1}{\kappa^2}$	$x_1=g-\Gamma-\frac{1}{2}$
Lax-Louisell equations		$x_1=\left[\left[\dfrac{g}{2}+\dfrac{\Gamma}{\kappa^2}\right]^2+\dfrac{2g}{\kappa^2}(g-\Gamma)\right]^{1/2}-\left[\dfrac{g}{2}+\dfrac{\Gamma}{\kappa^2}\right]$ $g_1=\left[\dfrac{1}{4}+\dfrac{\Gamma}{2}\right]\left[1+\left[1+\dfrac{4}{\kappa^2(\frac{1}{2}+\Gamma)}\right]^{1/2}\right]$	$x_1=g\left[\dfrac{g}{\frac{1}{2}+\Gamma}-1\right]$
Detuning and phase	$\Delta=0$	$\Delta=0$ $\phi_2=\pi,\ \phi_1=0$	$\Delta=\frac{1}{2}(\kappa^2 x_1-1)^{1/2}$ $\phi_2=0,\ \tan 2\phi_1=2\Delta,\ -\pi/2\le\phi_1\le 0$
$\alpha_1=q_1+iq_2$	$q_1=0,\ q_2=0$	$q_1=\sqrt{x_1},\ q_2=0$	$q_1=\sqrt{x_1}\cos\phi_1,\ q_2=\sqrt{x_1}\sin\phi_1$
$\alpha_2=q_3+iq_4$	$q_3=0,\ q_4=0$	$q_3=-\dfrac{\kappa}{2}x_1,\ q_4=0$	$q_3=\frac{1}{2}\sqrt{x_1},\ q_4=0$

$$\dot{\phi}_1 = -\Delta - \kappa \frac{x_4}{x_1} , \tag{9}$$

where the abbreviation

$$x_4 = \mathrm{Im}(\alpha_1^2 \alpha_2^*) = x_1 \sqrt{x_2} \sin(2\phi_1 - \phi_2) \tag{10}$$

is used.

The dynamical structure of the original equations (4) is hence determined by the reduced set of equations (8). These equations have three fixed points, which, along with their conditions of stability, are given in Table I in a compact form independent of the particular laser model. The fixed point (i), where the amplitudes in both modes vanish, is stable for pump rates $g < \Gamma$, i.e., the laser threshold is not changed by the presence of the nonlinear medium. The fixed points (ii) and (iii) are stable for $\Gamma < g < g_1$ and for $g > g_1$, respectively, where g_1 is given explicitly in Table I for both laser models.

However, a fixed point in the variables x_1, x_2, and x_3 is not necessarily a fixed point in the complex amplitudes α_1 and α_2. As follows from Eq. (9), a rotation with constant angular velocity $\dot{\phi}_1 = -\Delta - \kappa x_4 / x_1$ can be present. In the following, we will always assume that the detuning is $\Delta = -\kappa x_4 / x_1$, such that $\dot{\phi}_1 = 0$. Due to the phase symmetry, one of the phase angles ϕ_1 and ϕ_2 can be chosen arbitrarily. Here, we will choose $\phi_2 = \pi$ at the fixed point (ii) and $\phi_2 = 0$ at the fixed point (iii), which will simplify the calculations. Once ϕ_2 is specified, there is, in general, more than one possible value for ϕ_1, because the sign of the term $2\phi_1 - \phi_2$ is not determined by the values of x_1, x_2, and x_3. For the fixed point (ii), where $2\phi_1 - \phi_2 = \pm\pi$, this leads to physically identical solutions. For fixed point (iii), however, one obtains two physically distinct solutions that rotate with different angular velocities. In the following, we will consider only one of these solutions, making a choice for ϕ_1 and thus for the sign of x_4. With $\Delta = -\kappa x_4 / x_1$, this solution is described by stationary complex amplitudes α_1 and α_2.

Table I specifies the detuning Δ and the phase angles ϕ_1 and ϕ_2 at the three fixed points. For fixed point (iii), this implies that a choice of which of the two possible solutions is stationary has been made. Table I also contains the fixed-point values of the complex amplitudes α_1 and α_2, which can be calculated once the phase angles ϕ_1 and ϕ_2 are given, and which will be used in the next section.

B. Noise spectrum

For the calculation of the noise spectra, the quasi-Fokker-Planck equations (1) and (2) will be linearized around the fixed points of the classical dynamics given in Table I. We will use the notation $\alpha_1 = q_1 + iq_2$ and $\alpha_2 = q_3 + iq_4$. In scaled variables, the linearized equations for $P = P(q_1, q_2, q_3, q_4) = P(\{q_i\})$ can be written as

$$\frac{\partial P}{\partial \tau} = -\sum_{j,k=1}^{4} A_{jk}(\{\bar{q}_i\}) \frac{\partial}{\partial q_j}(q_k P) + \frac{1}{2}\frac{b}{\gamma_2} \sum_{j,k=1}^{4} D_{jk}(\{\bar{q}_i\}) \frac{\partial^2}{\partial q_j \partial q_k} P . \tag{11}$$

The matrices $A(\{\bar{q}_i\})$ and $D(\{\bar{q}_i\})$ are constant and depend only on the fixed-point values $\bar{q}_i$ given in Table I. The drift matrix A is given by

$$A(\{q_i\}) = \begin{bmatrix} f_g/2 + q_1^2 f_g' + \kappa q_3 & q_1 q_2 f_g' + \Delta + \kappa q_4 & \kappa q_1 & \kappa q_2 \\ q_1 q_2 f_g' - \Delta + \kappa q_4 & f_g/2 + q_2^2 f_g' - \kappa q_3 & -\kappa q_2 & \kappa q_1 \\ -\kappa q_1 & \kappa q_2 & -1 & 2\Delta \\ -\kappa q_2 & -\kappa q_1 & -2\Delta & -1 \end{bmatrix} . \tag{12}$$

For the diffusion matrix D, one obtains the block matrix

$$D(\{q_i\}) = \begin{bmatrix} D_A & 0 \\ 0 & 0 \end{bmatrix} \quad \text{where } D_A = \frac{\kappa}{2} \begin{bmatrix} q_3 & q_4 \\ q_4 & -q_3 \end{bmatrix} + D^L(q_1, q_2) , \tag{13}$$

and where the particular laser model enters through the laser diffusion-matrix D^L,

$$D^L(q_1, q_2) = \begin{bmatrix} g & 0 \\ 0 & g \end{bmatrix} \quad \text{(Haken-Lamb)} \tag{14}$$

or

$$D^L(q_1, q_2) = \left[1 + \frac{1}{g}(q_1^2 + q_2^2)\right]^{-2} \begin{bmatrix} g + q_1^2 & -q_1 q_2 \\ -q_1 q_2 & g + q_2^2 \end{bmatrix} \quad \text{(Lax-Louisell)} . \tag{15}$$

In these matrices, $f_g = f_g(q_1^2 + q_2^2)$ and $f_g' = f_g'(q_1^2 + q_2^2)$. The normalization of D is chosen such that D depends only on scaled variables. Since Eq. (11) describes an Ornstein-Uhlenbeck process,[25] there are analytic expressions for the noise spectra outside the cavity.[26,27] With the following definition of the spectral matrix $S(\Omega)$:

$$S(\Omega) = (A + i\Omega \mathbf{1})^{-1} D (A^T - i\Omega \mathbf{1})^{-1} , \tag{16}$$

the noise spectrum of the lasing mode in a quadrature

component with phase angle θ is

$$S_\theta(\Omega)=8\Gamma\{(\cos^2\theta)S_{11}(\Omega)+(\sin^2\theta)S_{22}(\Omega) +2(\sin\theta)(\cos\theta)[S_{12}(\Omega)+S_{21}(\Omega)]\} , \quad (17)$$

whereas for the second-harmonic mode,

$$S_\theta(\Omega)=8\{(\cos^2\theta)S_{33}(\Omega)+(\sin^2\theta)S_{44}(\Omega) +2(\sin\theta)(\cos\theta)[S_{34}(\Omega)+S_{43}(\Omega)]\} . \quad (18)$$

The factor Γ is absent in the last formula, because the damping rate for the second harmonic was scaled to 1. The spectra are normalized such that $S_\theta(\Omega)=0$ is the shot-noise level and $S_\theta(\Omega)=-1$ corresponds to perfect squeezing. Since $q_2=q_4=0$ at the fixed point (ii), the spectral matrix can be easily calculated for $\Gamma<g<g_1$. For those matrix elements which appear in Eqs. (17) and (18) one obtains

$$S_{11}(\Omega)=\frac{(D_{11}^L-\kappa^2x_1/4)(1+\Omega^2)}{[x_1(\kappa^2-f_g')-\Omega^2]^2+\Omega^2(x_1f_g'-1)^2} ,$$

$$S_{22}(\Omega)=\frac{(D_{22}^L+\kappa^2x_1/4)(1+\Omega^2)}{\Omega^2[\Omega^2+(\kappa^2x_1-1)^2]}$$

$$S_{33}(\Omega)=\frac{(D_{11}^L-\kappa^2x_1/4)\kappa^2x_1}{[x_1(\kappa^2-f_g')-\Omega^2]^2+\Omega^2(x_1f_g'-1)^2} , \quad (19)$$

$$S_{44}(\Omega)=\frac{(D_{22}^L+\kappa^2x_1/4)\kappa^2x_1}{\Omega^2[\Omega^2+(\kappa^2x_1-1)^2]} ,$$

$$S_{12}=S_{21}=S_{34}=S_{43}=0 .$$

Since for both laser models $D_{11}^L>0$ and $D_{22}^L>0$, only S_{11} and S_{33} can become negative. This means that, if there is any squeezing in this parameter range, it is maximal for $\theta=0$, i.e., it is amplitude squeezing. Due to the free phase diffusion, S_{22} and S_{44} diverge for $\Omega\to0$.

It is much harder to calculate the spectral matrix $S(\Omega)$ at the fixed point (iii), because q_2 does not vanish there. The calculation was done using the algebraic manipulation program REDUCE and leads to unwieldy expressions for $S(\Omega)$. They will be omitted as well as the results at the trivial fixed point (i), where there is no coherent excitation.

In the next two sections, a numerical analysis of the spectra at the fixed points (ii) and (iii) is given, based on the Haken-Lamb and Lax-Louisell laser models, respectively. Since outside the cavity the strongest squeezing is expected in the up-converted mode—which is confirmed by the explicit calculation—results will be presented only for this mode. In the lasing mode, less squeezing occurs outside the cavity because the spectrum Eq. (17) is multiplied by the laser threshold Γ which has to be chosen small in order to maximize the squeezing.[17,20,21] This is physically reasonable, since a low laser threshold means low spontaneous-emission noise.

C. Haken-Lamb model

The self-frequency-doubling laser based on the Haken-Lamb model has already been discussed in Ref. 17.

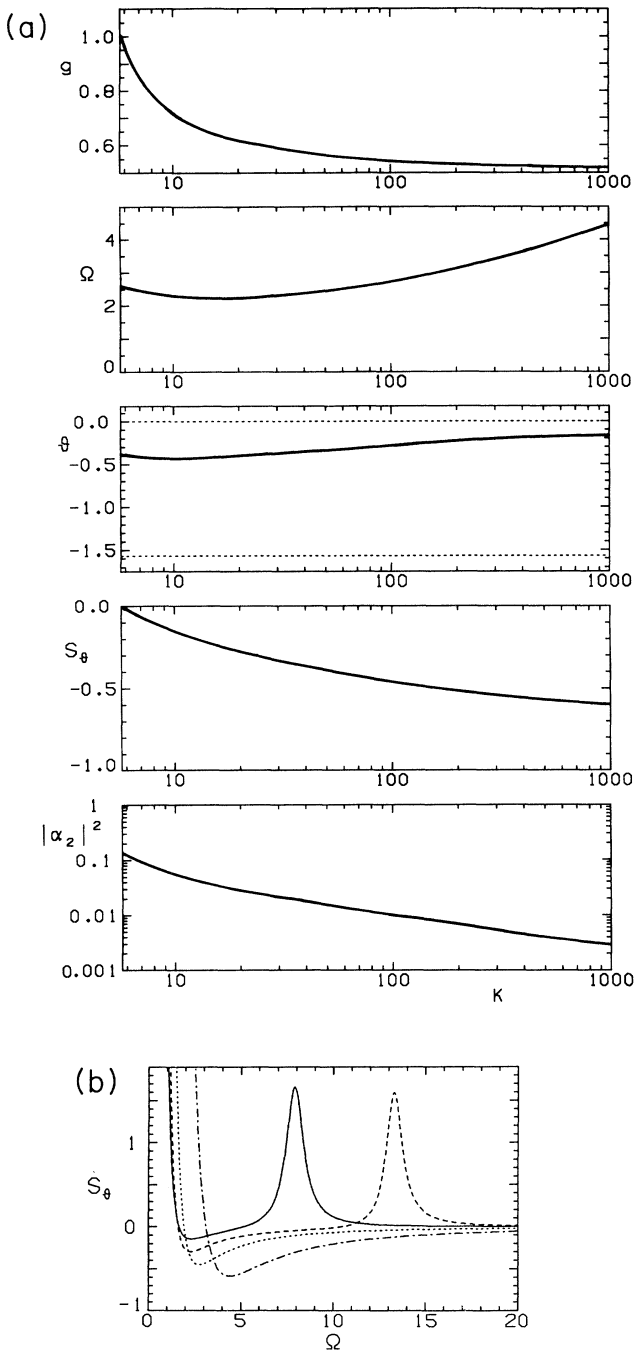

FIG. 1. Self-frequency-double laser, based on the Haken-Lamb laser theory, where squeezing occurs only at the fixed point (iii). The laser threshold is $\Gamma=10^{-2}$. All variables are given in scaled dimensionless units. (a) From top to bottom, the following five variables are shown as a function of the nonlinear coupling κ: the values of the pump rate g, the frequency offset Ω, and the phase angle θ, for which maximum squeezing occurs, the resulting value of the spectrum $S_\theta(\Omega)$; and the fixed-point value $|\alpha_2|^2$. The horizontal dotted lines indicate pure amplitude ($\theta=0$) and pure phase squeezing ($\theta=\pi/2$). (b) Noise spectra for the coupling constants $\kappa=10$ (solid line), $\kappa=25$ (dashed line), $\kappa=100$ (dotted line), and $\kappa=1000$ (dashed-dotted line). For g and θ, the optimized values of (a) are used.

There it was found that squeezing is possible only for $g > g_1$, i.e., at the fixed point (iii), and only if the condition

$$\kappa^2 > 32(1+\Gamma) \tag{20}$$

is fulfilled. Thus, a large nonlinear coupling κ and a low laser threshold Γ are required.

In Figs. 1(a) and 1(b), the largest possible squeezing in the second-harmonic mode outside the cavity at fixed point (iii) is shown for various values of κ, with the laser threshold fixed at $\Gamma = 10^{-2}$. In order to find the maximum squeezing for a given κ, Eq. (18) has been optimized with respect to the pump parameter g, the offset frequency Ω, and the phase angle θ. Figure 1(a) displays these optimized parameters along with the resulting maximum value of $S_\theta(\Omega)$ and the fixed-point value $|\alpha_2|^2$, which is a measure of the (scaled) intracavity photon number and thus of the brightness of the squeezed light outside the cavity. The spectra for different values of κ are shown in Fig. 1(b).

The κ value at the left edge of Fig. 1(a), where the squeezing vanishes, is given by Eq. (20). The squeezing increases with κ but never exceeds 65%. The phase angle θ decreases for large κ, which means that amplitude squeezing is approached. The divergence at $\Omega \to 0$ in Fig. 1(b) was already explained in the last section. The additional peaks in the spectra, which occur at offset frequencies $\Omega_{\max}$ that increase with κ, have their origin in the dynamics around fixed point (iii), where the stability matrix A has a pair of complex-conjugate eigenvalues. One can show that $\Omega_{\max}$ is equal to the modulus of the imaginary part of those eigenvalues. Analogous maxima can be found in the case of externally pumped frequency doubling.[24]

D. Lax-Louisell model

If the laser model of Lax and Louisell is used, basically the same picture as before arises. The main difference between both approaches results from the different behavior of the diffusion matrix D^L. Whereas in the Haken-Lamb case the matrix elements of D^L increase linearly with the pump strength g, here they tend to finite values of the order of the laser threshold Γ if $g \to \infty$. From this it follows that there exists no pump rate $g_{\max}$ where the squeezing is maximum. The squeezing increases monotonically with g.

This is why in Fig. 2(a) the coupling $\kappa = 5$ is held fixed, while g varies along the abscissa. The offset frequency Ω and the phase angle θ are chosen to maximize the squeezing. The vertical dashed line marks the threshold value $g = g_1$, which separates the stability domains of the fixed points (ii) and (iii). Again, squeezing occurs only at the fixed point (iii). With increasing pump rate g, the noise reduction rapidly approaches a limiting value of about 70%. Three typical spectra are displayed in Fig. 2(b). The situation closely resembles the Haken-Lamb case, with the exception that the maximum squeezing is now obtained for a smaller coupling parameter κ, and that it occurs over a large range of the pump rate g. From this it follows that in the particular experimental situation envisaged in Ref. 17, where almost no squeezing was found using the Haken-Lamb model, the analysis based on Lax and Louisell predicts that 60% squeezing can easily be obtained.

For larger κ, the picture does not change much. In

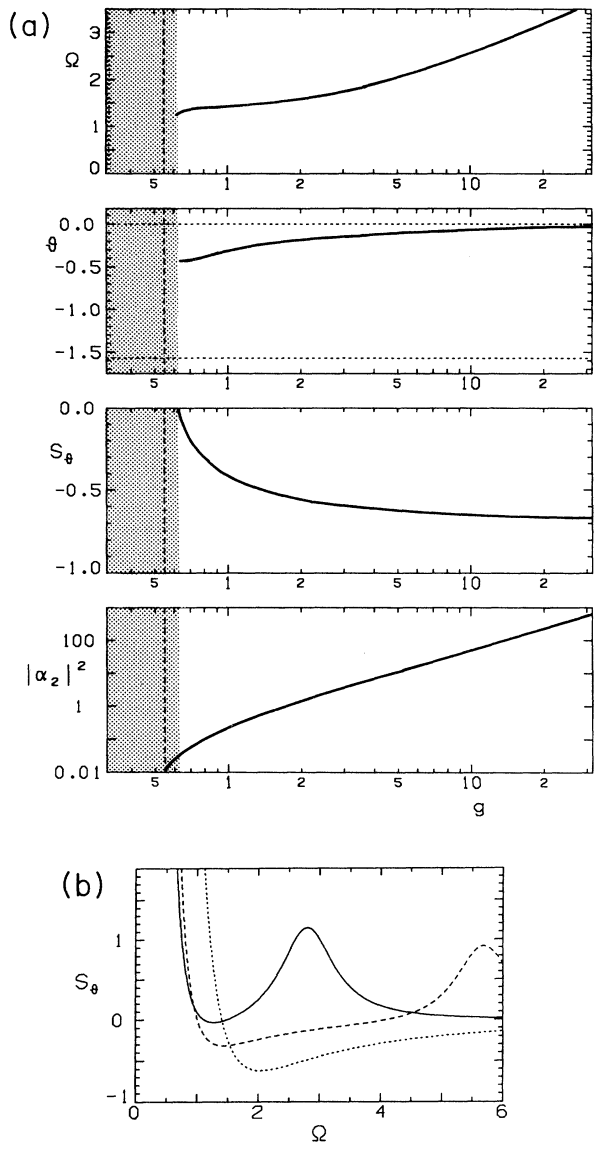

FIG. 2. Self-frequency doubling laser, based on the Lax-Louisell laser theory. $\kappa = 5$, $\Gamma = 10^{-2}$. (a) From top to bottom, the following four variables are shown as a function of the pump rate g: the values of Ω and θ for which maximum squeezing occurs, the resulting values of $S_\theta(\Omega)$, and the fixed-point value $|\alpha_2|^2$. The vertical dashed line indicates the boundary $g = g_1$ between fixed points (ii) and (iii). In the shaded area no squeezing occurs. (b) Noise spectra for the pump rates $g = 0.62$ (solid line), $g = 0.8$, (dashed line), and $g = 5$ (dotted line). For θ the optimized value of (a) is used.

particular, the maximum squeezing value of 70% is not exceeded even for a very large κ. This value can also be obtained for small κ, if higher pump rates g are allowed for, as can be seen from Fig. 3, where $\kappa=10^{-1}$. In this case, squeezing is also found at the fixed point (ii), where the optimized phase angle is $\theta=0$, which means pure amplitude squeezing. At the critical point $g=g_1$, a maximum of 50% noise reduction can be obtained in the limit $\kappa\to 0$. However, the necessary pump strength diverges in this limit, as follows from the explicit expressions Eqs. (18) and (19). Inserting the fixed-point values from Table I for $g=g_1$, one obtains

$$S_{\theta=0}(\Omega=0)|_{g=g_1}=8S_{33}(\Omega=0)|_{g=g_1}\to -0.5 \quad (\kappa\to 0 \text{ or } g_1\to\infty) \tag{21}$$

III. SELF-DOWN-CONVERTING LASER

In the self-down-converting laser, the high-frequency mode with amplitude α_2 is the lasing mode, which is then down-converted to the subharmonic with amplitude α_1. Equations (1) and (2) are easily modified in order to describe this new model. One obtains in the Haken-Lamb case

$$\frac{\partial P}{\partial t}=\left[-\frac{\partial}{\partial\beta_1}[\beta_1(-\gamma_1-i\delta_1)+\chi\beta_1^*\beta_2]+\text{c.c.}\right]P-\left[\frac{\partial}{\partial\beta_2}\left[\beta_2(\tilde{g}-\gamma_2-i\delta_2-b|\beta_2|^2)-\frac{\chi}{2}\beta_1^2\right]+\text{c.c.}\right]P$$
$$+\left[2\tilde{g}\frac{\partial^2}{\partial\beta_2\partial\beta_2^*}+\frac{\chi}{2}\left[\frac{\partial^2}{\partial\beta_1^2}\beta_2+\text{c.c.}\right]\right]P\ , \tag{22}$$

and in the Lax-Louisell case

$$\frac{\partial P}{\partial t}=\left[-\frac{\partial}{\partial\beta_1}[\beta_1(-\gamma_1-i\delta_1)+\chi\beta_1^*\beta_2]+\text{c.c.}\right]P$$
$$-\left\{\frac{\partial}{\partial\beta_2}\left[\beta_2\left[\frac{\tilde{g}}{1+b|\beta_2|^2/\tilde{g}}-\gamma_2-i\delta_2\right]-\frac{\chi}{2}\beta_1^2\right]+\text{c.c.}\right\}P+\left[\frac{\chi}{2}\frac{\partial^2}{\partial\beta_1^2}\beta_2+\text{c.c.}\right]P$$
$$+\left[-\frac{1}{2}\left[\frac{\partial^2}{\partial\beta_2^2}\frac{b\beta_2^2}{(1+b|\beta_2|^2/\tilde{g})^2}+\text{c.c.}\right]+\frac{\partial^2}{\partial\beta_2\partial\beta_2^*}\left[\frac{2\tilde{g}+b|\beta_2|^2}{(1+b|\beta_2|^2/\tilde{g})^2}\right]\right]P\ . \tag{23}$$

As above, it is assumed that $\delta_2=2\delta_1$. The time t will be scaled with the cavity damping rate γ_1 for the nonlasing mode. The scaled variables are

$$\tau=\gamma_1 t,\quad \alpha_i=\sqrt{b/\gamma_1}\beta_i\quad (i=1,2)\ ,$$
$$\Gamma=\frac{\gamma_2}{\gamma_1},\quad g=\frac{\tilde{g}}{\gamma_1},\quad \Delta=\frac{\delta_1}{\gamma_1}=\frac{\delta_2}{2\gamma_1},\quad \kappa=\frac{\chi}{\sqrt{b\gamma_1}}\ . \tag{24}$$

In the next section, the drift terms of Eqs. (23) and (24) will be examined.

A. Classical dynamics

The classical equations of motion equivalent to the drift parts of Eqs. (23) and (24) are

$$\dot{\alpha}_1=-(1+i\Delta)\alpha_1+\kappa\alpha_1^*\alpha_2\ ,$$
$$\dot{\alpha}_2=[\tfrac{1}{2}f_g(|\alpha_2|^2)-2i\Delta]\alpha_2-\frac{\kappa}{2}\alpha_1^2\ , \tag{25}$$

where f_g is defined in Eqs. (5) and (6). Since Eqs. (25) exhibit the same phase symmetry as Eqs. (4) for the self-frequency-doubling laser, they can be transformed using the same reduced set of variables Eqs. (7). One obtains

$$\dot{x}_1=-2x_1+2\kappa x_3\ ,$$
$$\dot{x}_2=f_g(x_2)x_2-\kappa x_3\ , \tag{26}$$
$$\dot{x}_3=[\tfrac{1}{2}f_g(x_2)-2]x_3+2\kappa x_1x_2-\frac{\kappa}{2}x_1^2\ .$$

The phase ϕ_1 obeys Eq. (9). The system of Eqs. (26) has four fixed points, which are displayed in Table II. As before, the laser threshold is $g=\Gamma$. The fixed point (iv) is completely analogous to the fixed point (iii) for frequency doubling, where the same condition $f_g=\text{const}$ holds. Again, a rotation is present, which is treated in the same way as before (see Table II). The main difference in the dynamical structure of Eqs. (8) and (26) appears for moderate pump rates g. The intermediate range now splits into two fixed points. In the domain of stability of fixed point (ii), there is lasing action in the high-frequency mode ($x_2>0$), but there is no conversion into the low-frequency mode ($x_1=0$). In this domain, the classical dynamics behaves as if the nonlinear crystal were not present. The fixed point (ii) is stable until, at the pump rate $g=g_1$, the threshold value $x_2=1/\kappa^2$ is reached. If the pump rate is increased further, the fixed point (iii) becomes stable. Now x_2 remains constant and the addi-

TABLE II. Self-down converting laser model characteristics for four fixed points.

Feature	Fixed point (i)	Fixed point (ii)	Fixed point (iii)	Fixed point (iv)
Stability range	$g<\Gamma$	$\Gamma<g<g_1$	$g_1<g<g_2$	$g>g_3$
Defining equations	$x_1=0$ $x_2=0$ $x_3=0$	$x_1=0$ $f_g(x_2)=0$ $x_3=0$	$x_1=x_2 f_g(x_2)$ $x_2=1/\kappa^2$ $x_3=\frac{1}{\kappa}x_2 f_g(x_2)$	$x_1=4x_2$ $f_g(x_2)=4$ $x_3=\frac{4}{\kappa}x_2$
Stability conditions	$f_g(x_2)<0$	$0<x_2<\frac{1}{\kappa^2}$	$0<f_g(x_2)<4$ $f_g'(x_2)<-\frac{\kappa^2}{2}f_g(x_2)$	$x_2>1/\kappa^2$ $f_g'(x_2)<-\frac{3}{x_2}\frac{\kappa^2 x_2-\frac{2}{3}}{\kappa^2 x_2-\frac{1}{2}}$
Haken-Lamb equations		$x_2=g-\Gamma$ $g_1=\Gamma+\frac{1}{\kappa^2}$	$f_g(x_2)=2(g-\Gamma-x_2)$ $g_2=\Gamma+\min\left[\frac{3}{\kappa^2},2+\frac{1}{\kappa^2}\right]$	$x_2=g-\Gamma-2$ $g_3=\Gamma+\max\left[2+\frac{1}{\kappa^2},\frac{11}{4}+\frac{1}{4\kappa^2}+\left[\frac{9}{16}+\frac{1}{16\kappa^4}-\frac{5}{8\kappa^2}\right]^{1/2}\right]$
Lax-Louisell equations		$x_2=\frac{g}{\Gamma}(g-\Gamma)$ $g_1=\frac{\Gamma}{2}\left[1+\left[1+\frac{4}{\kappa^2\Gamma}\right]^{1/2}\right]$	$f_g(x_2)=\frac{2g}{1+x_2/g}-2\Gamma$ g_2 (see text)	$x_2=g\left[\frac{g}{2+\Gamma}-1\right]$ g_3 (see text)
Detuning and phase		$\Delta=0$ $\phi_1=0,\ \phi_2=0$	$\Delta=0$ $\phi_1=0,\ \phi_2=0$	$\Delta=(\kappa^2 x_2-1)^{1/2}$ $\phi_1=0,\ \tan\phi_2=\Delta,\ 0\le\phi_2\le\pi/2$
$\alpha_1=q_1+iq_2,$	$q_1=0,\ q_2=0$	$q_1=0,\ q_2=0$	$q_1=\frac{1}{\kappa}\sqrt{f_g(x_2)},\ q_2=0$	$q_1=2\sqrt{x_2},\ q_2=0$
$\alpha_2=q_3+iq_4$	$q_3=0,\ q_4=0$	$q_3=\sqrt{x_2},\ q_4=0$	$q_3=\frac{1}{\kappa},\ q_4=0$	$q_3=\frac{1}{\kappa},\ q_4=\frac{\Delta}{\kappa}$

tional pump power is entirely converted into mode 1. The upper limit of stability $g=g_2$ of the fixed point (iii) as well as the lower limit of stability $g=g_3$ of fixed point (iv) depend on the details of the function $f_g(x_2)$ and of its derivative $f_g'(x_2)$ and thus on the details of the particular laser model used.

For the Haken-Lamb laser model, g_2 and g_3 are given explicitly in Table II. If the nonlinear coupling is $\kappa>1$, one finds $g_2<g_3$, and thus a domain where no stable fixed point exists, whereas for $\kappa\leq 1$, one has $g_2=g_3=2+1/\kappa^2$, and no stability gap occurs. Numerical integration of the equations of motion in the case $\kappa>1$ shows that a stable limit cycle exists for $g_2<g<g_3$. This means that self-pulsing can be expected in the self-down-converting laser if the pump rate is increased beyond $g=g_2$. For pump rates $g>g_3$, the laser should become stable again. A similar self-pulsing has been predicted for externally pumped second-harmonic generation,[24] but has not been observed experimentally up to the present time.

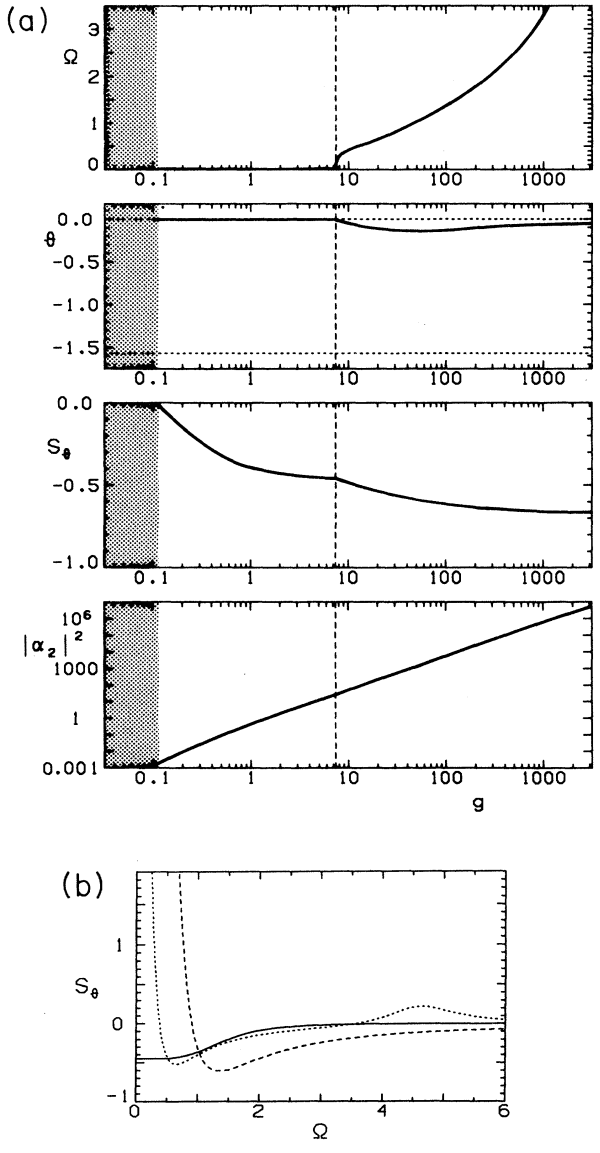

FIG. 3. As in Fig. 2, but $\kappa=10^{-1}$. (a) As in Fig. 2(a). (b) $g=7.4$ (solid line), $g=20$ (dotted line), and $g=100$ (dashed line), with optimized θ.

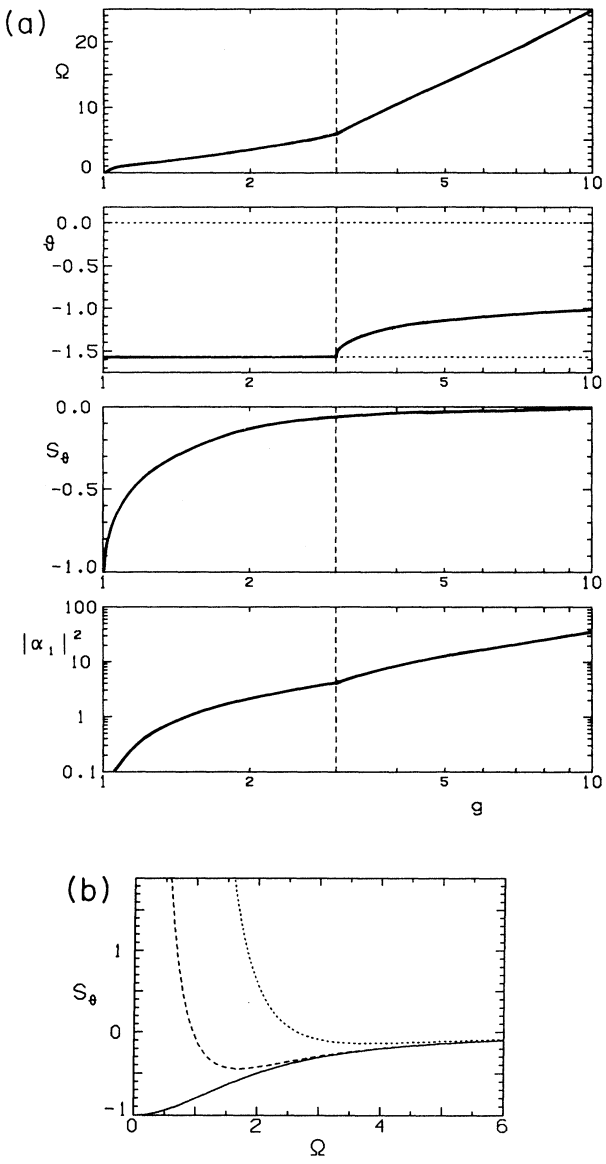

FIG. 4. Self-down-converting laser, based on the Haken-Lamb laser theory. $\kappa=1$, $\Gamma=10^{-4}$. (a) From top to bottom, the following four variables are shown as a function of the pump rate g: the values of Ω and θ for which maximum squeezing occurs, the resulting value of $S_\theta(\Omega)$, and the fixed-point value $|\alpha_1|^2$. The vertical dashed line indicates the boundary $g=g_2=g_3$ between fixed points (iii) and (iv). (b) Noise spectra for the pump rates $g=g_1=1.0001$ (solid line), $g=1.2$ (dashed line), and $g=2$ (dotted line), with optimized θ.

In the case of the Lax-Louisell laser model, the expressions for g_2 and g_3 are too complicated to be shown explicitly. Numerically, one finds that $g_2=g_3$ for $\kappa<0.406$. In the limit $\Gamma\to 0$, the condition of stability of fixed point (iii) simplifies to

$$\kappa^2 f_g(x_2)<1 , \tag{27}$$

and the expression for the threshold g_2 becomes

$$g_2\simeq\min[1/\kappa^2, 1+\sqrt{1+(2/\kappa^2)}] \quad (\Gamma\to 0) . \tag{28}$$

In this limit, the upper threshold converges to $g_3\simeq 8$ for $\kappa>5$.

B. Noise spectrum

After linearization, Eqs. (22) and (23) can be written in the unified form

$$\frac{\partial P}{\partial\tau}=-\sum_{j,k=1}^{4} A_{jk}(\{\bar{q}_i\})\frac{\partial}{\partial q_j}(q_k P) + \frac{1}{2}\frac{b}{\gamma_1}\sum_{j,k=1}^{4} D_{jk}(\{\bar{q}_i\})\frac{\partial^2}{\partial q_j\partial q_k}P , \tag{29}$$

where the drift and diffusions matrices are given by

$$A(\{q_i\})=\begin{bmatrix} -1+\kappa q_3 & \Delta+\kappa q_4 & \kappa q_1 & \kappa q_2 \\ -\Delta+\kappa q_4 & -1-\kappa q_3 & -\kappa q_2 & \kappa q_1 \\ -\kappa q_1 & \kappa q_2 & f_g/2+q_3^2 f_g' & q_3 q_4 f_g'+2\Delta \\ -\kappa q_2 & -\kappa q_1 & q_3 q_4 f_g'-2\Delta & f_g/2+q_4^2 f_g' \end{bmatrix} \tag{30}$$

and

$$D(\{q_i\})=\begin{bmatrix} D_A & 0 \\ 0 & D^L(q_3,q_4) \end{bmatrix} \text{ with } D_A=\frac{\kappa}{2}\begin{bmatrix} q_3 & q_4 \\ q_4 & -q_3 \end{bmatrix} . \tag{31}$$

In these matrices, $f_g=f_g(q_3^2+q_4^2)$ and $f_g'=f_g'(q_3^2+q_4^2)$.

As before, a low laser threshold Γ will be assumed, such that large noise reduction outside the resonator can occur in the converted mode, which is the low-frequency mode here. Since there is no coherent excitation in this mode for $g<g_1$, the discussion will focus on the domain $g\geq g_1$, i.e., on the fixed points (iii) and (iv), where bright squeezing in mode 1 is possible.

Whereas for fixed point (iv) the expressions for the spectral matrix are very unwieldy, they are easy to calculate at fixed point (iii), where $q_2=q_4=0$. For $g_1<g<g_2$, the matrix elements that appear in Eqs. (17) and (18) are

$$\begin{aligned} S_{11}(\Omega)&=\left[f_g D_{11}^L+\frac{\Omega^2}{2}+\frac{1}{2}\left[\frac{f_g}{2}+\frac{f_g'}{\kappa^2}\right]^2\right]\Big/\left[(f_g-\Omega^2)^2+\Omega^2\left[\frac{f_g}{2}+\frac{f_g'}{\kappa^2}\right]^2\right] , \\ S_{22}(\Omega)&=\left[f_g D_{22}^L-\frac{1}{2}\left[\frac{f_g^2}{4}+\Omega^2\right]\right]\Big/\{\Omega^2[\Omega^2+(2-f_g/2)^2]\} , \\ S_{22}(\Omega)&=\left[\Omega^2 D_{11}^L+\frac{f_g}{2}\right]\Big/\left[(f_g-\Omega^2)^2+\Omega^2\left[\frac{f_g}{2}+\frac{f_g'}{\kappa^2}\right]^2\right] , \\ S_{44}(\Omega)&=\left[(4+\Omega^2)D_{22}^L-\frac{f_g}{2}\right]\Big/\{\Omega^2[\Omega^2+(2-f_g/2)^2]\} , \\ S_{12}&=S_{21}=S_{34}=S_{43}=0 . \end{aligned} \tag{32}$$

Since for both laser models $D_{11}^L>0$ and $D_{22}^L>0$, only S_{22} and S_{44} can become negative. This means that if there is any squeezing, it is maximal at the phase angle $\theta=\pi/2$, i.e., it is phase squeezing. For $g=g_1$, at the lower stability limit of fixed point (iii), one finds in the low-frequency mode

$$S_{\pi/2}(\Omega)=-\frac{4}{\Omega^2+4} . \tag{33}$$

This means 100% noise reduction at the center frequency $\Omega=0$. Since $x_1=0$ at $g=g_1$, the resulting state is a squeezed vacuum state. For $g>g_1$, a coherent amplitude develops ($x_1>0$), but the maximum squeezing decreases. The Haken-Lamb and the Lax-Louisell cases will be discussed separately in the following sections.

C. Haken-Lamb model

Results of the numerical analysis of the noise spectra in the low-frequency mode are shown in Fig. 4 for a nonlinear coupling $\kappa=1$. The data are displayed in a way analogous to Figs. 2 and 3. The vertical dashed line in

Fig. 3(a) indicates the threshold value $g=g_2=g_3$, i.e., the boundary between fixed points (iii) and (iv). For $\kappa=1$ there is no stability gap. At the pump rate $g=g_1$, at the left edge of Fig. 3(a), there is 100% noise reduction in the vacuum state. This maximum value is obtained at $\theta=\pi/2$ and $\Omega=0$. If the pump rate is increased, a coherent amplitude $|\alpha_1|^2>0$ develops, but at the same time the maximum squeezing decreases. However, for moderate brightness, large noise reduction can still be achieved. In contrast to the case of frequency doubling, nothing is gained here by increasing the pump rate into the domain of the last stable fixed point. Three typical spectra are displayed in Fig. 4(b). For larger values of κ, the situation remains essentially the same. Apart from the stability gap, the main difference is that the same amount of squeezing is now obtained at lower pump rates.

D. Lax-Louisell model

In Fig. 5, the analysis of the case $\kappa=1$ of the last section is repeated for the Lax-Louisell laser model. In this case, $g_2<g_3$,and a stability gap between fixed points (iii)

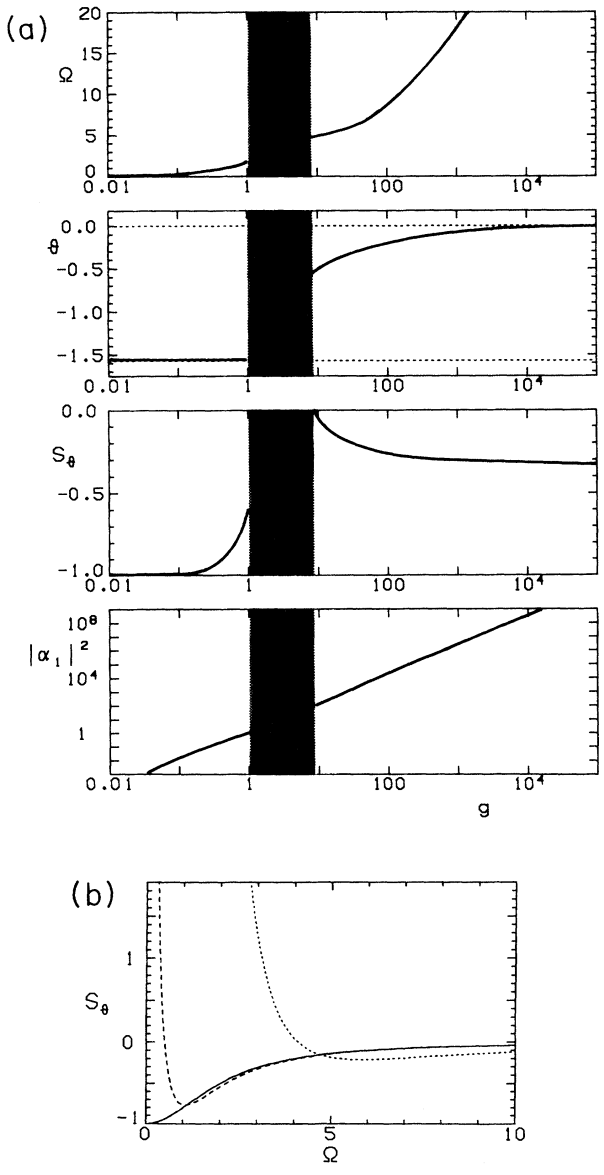

FIG. 5. Self-down-converting laser, based on the Lax-Louisell laser theory. $\kappa=1$, $\Gamma=10^{-4}$. (a) As in Fig. 4(a). The shaded area indicates the stability gap $g_2<g<g_3$ between the fixed points (iii) and (iv). (b) $g=g_1=0.0101$ (solid line), $g=0.7$ (dashed line), and $g=30$ (dotted line), with optimized θ.

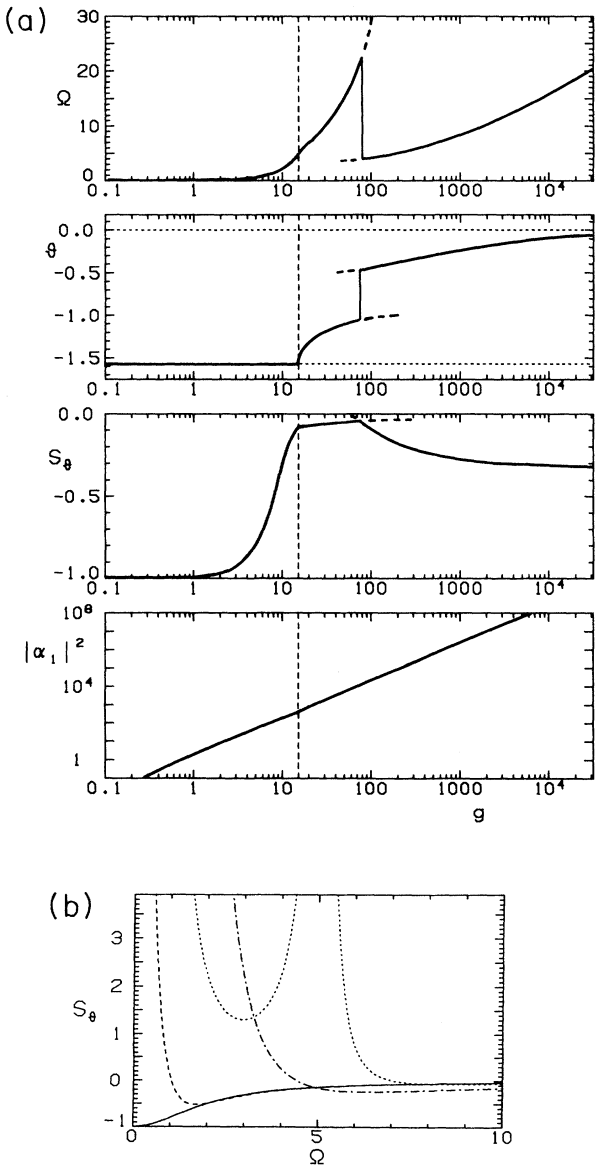

FIG. 6. As in Fig. 5, but $\kappa=10^{-1}$. (a) As in Fig. 4(a). (b) $g=g_1=0.101$ (solid line), $g=8$ (dashed line), $g=25$ (dotted line), and $g=400$ (dashed-dotted line), with optimized θ.

and (iv) exists. The unstable range $g_2 < g < g_3$ is indicated by the shaded area in Fig. 5(a). In the range $g_1 < g < g_2$, in the left part of Fig. 5(a), the situation is similar to the Haken-Lamb case. Here, the maximum squeezing is found at smaller offset frequencies Ω and decreases less rapidly with the pump rate. For $g > g_3$, however, at the fixed point (iv), a new feature appears. There is no squeezing at the right edge $g = g_3$ of the stability gap, but the maximum squeezing increases monotonically with the pump rate g to reach a limiting vaue of about 35%. The phase angle θ decreases with g, which means that amplitude squeezing is approached. Three typical spectra are displayed in Fig. 5(b).

No changes occur in principle when a different coupling constant κ is used. It is found that a large κ requires smaller pumping rates to achieve the same amount of noise reduction. The case $\kappa = 10^{-1}$, where no stability gap appears, is shown in Fig. 6. There is a slight complication here due to the additional peak in the spectrum. This peak was already discussed in Sec. II C. For pump rates close to the boundary $g = g_3$, this peak occupies just the place where otherwise the spectral-noise minimum would be [see the dotted curve in Fig. 6(b)]. This means that the offset frequency where the maximum squeezing occurs is pushed to higher values. Figure 6(b) shows that, with increasing pump rate, the additional peak moves to the right, such that for a certain pump rate g, the location of the maximum squeezing jumps to the left. This is the reason for the discontinuities in Fig. 6(a). Apart from this peculiarity, the behavior is similar to the case $\kappa = 1$.

IV. CONCLUSION

Incoherently pumped lasers with an intracavity $\chi^{(2)}$-nonlinear element can generate intense squeezed subharmonic or second-harmonic light. We have found that the amount of squeezing is limited due to the laser phase noise, which shows up as excess noise in a narrow band around the central frequency, and which pushes the maximum spectral squeezing away from the center frequency into the sidebands. In the limit of large pump rates, the nonlinear dynamics leads to a bifurcation and to rotating field vectors, which tilt the squeezing ellipse. For this reason there exists no pure phase or amplitude squeezed state in this limit.

For the self-down-converting laser, 100% noise reduction is possible at the second threshold, where the conversion to the subharmonic mode starts. Just at this threshold, the subharmonic mode is still in the vacuum state. In the limit of large pump rates, a maximum of about 30% squeezing can be achieved.

More than 60% noise reduction at high pumping rates seems to be possible in the self-frequency-doubling laser. This limit is predicted irrespective of whether the analysis is based on the Haken-Lamb or the Lax-Louisell laser model. However, when the question of practical realization of such a device is addressed, both laser models lead to different answers. The application of our previous analysis using the Haken-Lamb model to a self-frequency-doubling laser made from Nd:MgO:$LiNbO_3$ suggested that no squeezing can be obtained from this particular device.[17] But if the Lax-Louisell model is used, one finds that 60% noise reduction can easily be achieved with this material.

Self-frequency-doubling lasers have been developed and are now commercially available.[28] Research has focused on diode-pumped devices using neodymium yttrium aluminum borate (NYAB) self-frequency-doubling crystals or the nonlinear crystal potassium titanyl phosphate (KTP) with lithium neodymium tetraphosphate (LNP) as lasing medium. In order to increase the conversion efficiency, the second-harmonic mode has been resonantly enhanced in the latter system.[29] Resonance for the second-harmonic mode is also essential for generating squeezed light. Even though the potential for squeezing seems to be limited to approximately 60%, there are several advantages combined in self-frequency-doubling lasers as sources of nonclassical light. They can be incoherently pumped, the squeezed mode is at the shorter wavelength, and the high power of the beam implies that the shot-noise level is low. For applications, e.g., in sub-shot-noise interferometric devices, these lasers could be a promising light source.

ACKNOWLEDGMENTS

One of us (A. Sizmann) acknowledges support from the European Community under Grant No. ST2J-0278-C (EDB) and Esprit Project no. 3186.

[1]Y. Yamamoto, S. Machida, and O. Nilsson, Phys. Rev. A **34**, 4025 (1986).

[2]S. Machida, Y. Yamamoto, and Y. Itaya, Phys. Rev. Lett. **58**, 1000 (1987).

[3]S. Machida and Y. Yamamoto, Phys. Rev. Lett. **60**, 792 (1988).

[4]W. H. Richardson, S. Machida, and Y. Yamamoto, in *International Conference on Quantum Electronics Technical Digest Series 1990* (Optical Society of America, Washington, DC, 1990), p. 395.

[5]D. F. Walls, Nature **306**, 141 (1983).

[6]R. E. Slusher, L. W. Hollberg, B. Yurke, J. C. Mertz, and J. F. Valley, Phys. Rev. Lett. **55**, 2409 (1985).

[7]R. M. Shelby, M. D. Levenson, S. H. Perlmutter, R. G. DeVoe, and D. F. Walls, Phys. Rev. Lett. **57**, 691 (1986).

[8]L.-A. Wu, H. J. Kimble, J. L. Hall, and H. Wu, Phys. Rev. Lett. **57**, 2520 (1986).

[9]Special Issue on Squeezed States of the Electromagnetic Field, edited by H. J. Kimble and D. F. Walls [J. Opt. Soc. Am. B **4**, 1450 (1987)].

[10]Special Issue on Squeezed Light, edited by R. Loudon and P. L. Knight [J. Mod. Opt. **34**, 709 (1987)].

[11]T. Debuisschert, S. Reynaud, A. Heidmann, E. Giacobino, and C. Fabre, Quantum Opt. **1**, 3 (1989).

[12]J. Mertz, A. Heidmann, C. Fabre, E. Giacobino, and S. Reynaud, Phys. Rev. Lett. **64**, 2897 (1990).

[13]A. Sizmann, R. J. Horowicz, G. Wagner, and G. Leuchs, Opt. Commun. **80**, 138 (1990).

[14]H. P. Yuen, Phys. Rev. A **13**, 2226 (1976).

[15]C. M. Caves, Phys. Rev. D **23**, 1693 (1981).

[16]R. Loudon and P. L. Knight, J. Mod. Opt. **34**, 709 (1987).

[17]A. Sizmann, R. Schack, and A. Schenzle, Europhys. Lett. **13**, 109 (1990).

[18]H. Haken, *Laser theory, Handbuch der Physik* Vol. XXV/2c (Springer, Berlin, 1970).
[19]M. Sargent, M. O. Scully, and W. E. Lamb, *Laser Physics* (Addison-Wesley, Reading, MA, 1974).
[20]V. N. Gorbachev and E. S. Polzik, Zh. Eksp. Teor. Fiz. **96**, 1984 (1989) [Sov. Phys.—JETP **69**, 1119 (1989)].
[21]D. F. Walls, M. J. Collett, and A. S. Lane, Phys. Rev. A **42**, 4366 (1990).
[22]W. H. Louisell, *Quantum Statistical Properties of Radiation* (Wiley, New York, 1973).
[23]H. Risken, in *Progress in Optics,* edited by E. Wolf (North-Holland, Amsterdam, 1970), Vol. 8, p. 241.
[24]P. D. Drummond, K. J. McNeil, and D. F. Walls, Opt. Acta **28**, 211 (1981).
[25]C. W. Gardiner, *Handbood of Stochastic Methods,* 2nd ed. (Springer, Berlin, 1985).
[26]C. W. Gardiner and M. J. Collett, Phys. Rev. A **31**, 3761 (1985).
[27]M. J. Collett and D. F. Walls, Phys. Rev. A **32**, 2887 (1985).
[28]G. J. Dixon, Laser Focus World, Sept. 1990, p. 99, and references therein.
[29]G. J. Dixon and S. G. Grubb, in *Conference on Lasers and Electro-Optics Technical Digest Series 1990* (Optical Society of America, Washington, DC, 1990), p. 680.